Chemical Bonding, Kinetics, and the Approach to Equilibrium Structures of Simple Metallic, Molecular, and Network Microclusters

J. C. PHILLIPS

AT&T Bell Laboratories, Murray Hill, New Jersey 07974

Received October 2, 1985 (Revised Manuscript Received March 6, 1986)

Contents

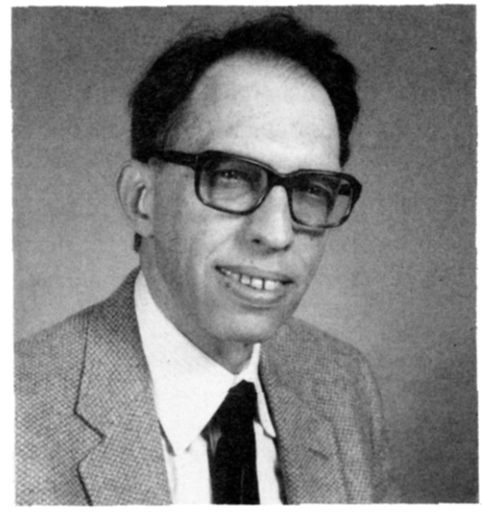

J. C. Phillips was born in 1933, in New Orleans. He received his Ph.D. in 1956, at the University of Chicago under M. H. Cohen. He studied at Bell Laboratories, the University of California at Berkeley, and Cambridge University before taking up a faculty position at the University of Chicago in 1960, where he became a full professor in 1965. In 1972 he received the Buckley Prize from the American Physical Society for his studies of chemical bonding in solids in the context of pseudopotential theory. In 1978 he was elected to the National Academy of Sciences. His quantum studies include systematic classification and prediction of crystal structures, and in the last decade he has discussed the material properties of solids with special emphasis on network glasses. His hobbies are chess, Go, and music.

I. Introduction

Rapid cooling or quenching of a gas of atoms or small molecules by adiabatic expansion can produce clusters of n atoms or molecules with average values of $n = \bar{n}$ with $\bar{n}$ of order 5 or 10. The simplest means of producing the gas is thermally either in an oven or by cathodic evaporation. An alternative method is pulsed laser evaporation, which may have technological appeal because of its capability of easy and rapid chemical analysis on a small scale in biological and industrial contexts, for example. Thus early interest in ion desorption mass spectrometry increased because the advent of lasers made possible a marriage between these two instruments leading to analytic sensitivities $\sim$100 times greater than that of the electron microprobe.[1] A menage á trois including a supersonically pulsed carrier gas has recently made possible the profuse production of microclusters containing $n = 10^2$ or more monomers per cluster.[2] Ion production efficiency is increased further by use of a second laser for ionization or neutral clusters. Photofragmentation branching ratios can be measured with a third laser, providing additional flexibility and insight into the kinetics of cluster formation.[3] With these advances in instrumentation cluster formation and growth has become a valid scientific subject in its own right, and is no longer merely a means to the end of providing a source for clusters or for use as a microanalytical probe. Further fundamental research on this subject offers interesting prospects, however, for enhancing the value of the laser microprobe in technological contexts.[1]

In early work a tendency to confine the analysis to small clusters with $n \lesssim 10$ is noticeable. Recent technical advances[2,3] suggest that much future research will explore the microcluster regime $10 \lesssim n \lesssim 1000$ where the transition from "molecular" to "solid" clusters takes place. In this regime peaks in ionized cluster concentrations $c_n^{\pm}$ have been observed for many materials. These relative abundance maxima (sometimes called "magic numbers") can be related in some cases to peaks in d^2E/dn^2, where E (n) is the cohesive energy of an n-monomer cluster. In other cases concentration peaks must depend on the kinetics of cluster formation and fragmentation, as the peak values of n vary from one laboratory to the next and sometimes even from one run to the next in the same laboratory.

It has been widely assumed that when the kinetics of cluster formation are such as to promote close approach to equilibrium, the relative abundance maxima reflect especially stable, or in some sense closed shell, structures. In a few especially favorable and simple

0009-2665/86/0786-0619$06.50/0

cases these structures can be inferred from simple atomic geometrical or electronic models. These cases correspond to the inert gas clusters and nearly free electron metallic clusters discussed in sections III and IV. However, a different picture is presented by clusters constructed from elements which form network structures in the solid phase. This is not surprising, because we know from kinetic studies of formation of network and metallic glasses that some of the former can be quenched as much as 10^9 times more slowly than the latter with avoidance of crystallization. Possible scenarios for large kinetic viscosities in coalescence and growth of network clusters are discussed in conjunction with a review of the data in section V.

To set the stage for the critical review of the competition between energetic and kinetic factors in determining microcluster concentration spectra, classical coagulation theory is discussed in section II. This theory may be applicable primarily to the growth of large molecular clusters, but it provides a convenient framework for discussing kinetic effects in general.

A word is appropriate here concerning cluster structure determinations. In the case of small clusters ($n < 10$) it may be possible to determine cluster structures independently of concentration spectra by direct methods, diffraction, infrared spectra, and so on. With increasing $n > 10$ sample density (for any specific n) decreases rapidly and so does the information contained in the direct measurement. Apart from concentration peaks other scalar properties such as ionization potential or electric or magnetic polarizabilities may be measured as function of n. So far these have been measured to a much smaller extent than the concentration profiles upon which the attention of this review is largely fixed.

In principle the cluster structure energies $E(n)$ can be calculated quantum-mechanically and this possibility makes microclusters an attractive subject for theorists. Indeed we may hope that microclusters may eventually prove a testing ground where theoretical quantum chemists and physicists may compare the relative merits of their various approaches. In making such comparisons (based on concentration peaks) it is important to be confident that these peaks are indeed reflections of equilibrium energies and not artifacts of the kinetics of cluster growth and ionization. Thus the present effort to identify and separate energetic and kinetic factors has both experimental and theoretical implications. At the same time we may expect that further advances in experimental technique will overcome some of the difficulties mentioned above and provide information in addition to that contained in concentration spectra. However, as we shall see, great progress has already been made in analyzing microcluster structure largely from concentration spectra alone. It is this progress which is the subject of the present review.

At this point I comment on how this review might be used by the reader. No effort has been made to produce an exhaustive review, which could easily contain more than 1000 references but which would still rapidly become obsolete in this expanding field. Instead I have chosen to discuss a certain selection of papers which I have found especially enjoyable and instructive reading. This review is not supposed to be self-contained, and the reader is directed to read the original papers cited for details not discussed here. To these papers my discussion adds theoretical analysis and ideas which have become possible at this time. Not all of these theoretical ideas are etched in granite, but none of them are frivolous, and I believe that because so little theoretical attention has been directed to this subject, many workers in the field will find my discussion stimulating.

It is important to bear in mind in these theoretical discussions that attention is focussed on the principal mechanisms that may be important to the observations. Prospects for rigorous quantum-mechanical calculations of structural energies, collision cross-sections and ionization fragmentation probabilities of all low-energy cluster configurations in the range $10 \leq n \leq 100$ are bleak. Yet many striking experimental results have been obtained already which can be discussed quantitatively with the comparatively simple theoretical ideas reviewed here.

The familiar divergence in taste between chemists and physicists becomes apparent in this field which has attracted workers from both disciplines. Inspection of the references given here shows that authors from both disciplines are nearly equally represented, an unusual situation. Just as I hope that physicists will find this article in this journal, so I also hope that chemists will not be reluctant to study both experiments and theory from physicists, although some elements of my presentation may be unfamiliar.

II. Classical Coagulation

When sample atoms first begin to condense as a result of adiabatic expansion of a gas, prepared continuously or following evaporation by a laser pulse, initially cluster growth proceeds via monomer addition. At later times the supply of monomers diminishes and eventually cluster growth takes place by fusion of large clusters into larger clusters. Kinetic equations to describe the transition from one regime to another are described in sections IIA and IIB. These equations are especially simple for a homosystem such as an inert gas. For a heterosystem such as sample plus cooling carrier gas the equations charge quantitatively but not qualitatively. Significant complications appear when we attempt to include concentration peaks and the effects of evaporation or fragmentation following ionization by an electron beam or later laser photons, as discussed in section IIC.

A. Kinetic Equations

We begin by assuming that the system is a pure condensing gas which initially consists of monomers, and that for all k-mers evaporation can be neglected compared to condensation. Then the kinetic equations for coagulation of k-size clusters read[4]

$$\frac{dn_k}{dt} = \sum_{\substack{i+j=k \\ i \leq j}} C_{ij}\, n_i n_j - \sum_i C_{ik}\, n_i n_k \qquad (1)$$

The rate coefficients, assuming thermal velocities for all k-mers and equal masses for all monomers, are

$$C_{ij} = 2\sigma_{ij}\left(\frac{2kT}{m\pi}\right)^{1/2}\left(\frac{i+j}{ij}\right)^{1/2} \qquad (2)$$

The important feature of (2) is that $C_{1j} \gg C_{ij}$ for $1 \ll$

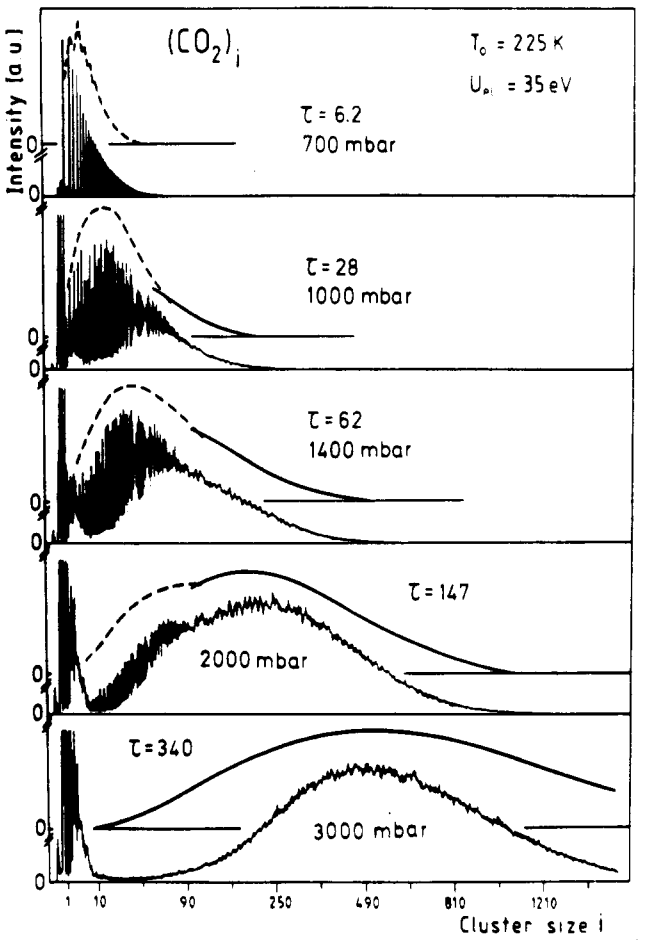

Figure 1. Mass spectra of CO_2 clusters for increasing stagnation pressures corresponding to dimensionless interaction interval parameters τ. Data from ref 4.

i. This means that in the early stages of cluster growth monomer addition dominates the kinetics because of fast thermal monomer motion. In (2) σ_{ij} is the cross-section, which is

$$\sigma_{ij} = f_{ij}\sigma_{ij}^{(0)} \tag{3}$$

where $\sigma_{ij}^{(0)}$ is the geometrical cross section, which is proportional to $(i^{1/3} + j^{1/3})^2$, and f_{ij} is the sticking coefficient. Assuming $f_{ij} = 1$ we obtain the classical limit that has been discussed extensively in connection with aerosol coagulation kinetics.[5]

The classical equations, when reduced to a universal form with the assumption $f_{ij} = 1$, can be solved numerically. All the solutions are specified by a parameter τ related to a kinetically weighted average of $T^{1/2}\rho$, where ρ is the gas density. In effect τ determines the median cluster size $\langle n_k \rangle$ after coagulation has been arrested by expansion, or it can be inferred from measured values of $\langle n_k \rangle$.

B. Transition from Monomer Addition to Fusion

In this way classical coagulation theory has been tested with values of $\langle n_k \rangle$ ranging between 5 and 500. The results for CO_2 gas after adiabatic expansion are shown in Figure 1, where τ is compared to the pressure in the chamber prior to expansion.[5]

The salient feature of the spectrum is that for small τ it has a Poisson character associated with monomer addition, with largest n_k for $k = 1$, and that for large $\langle n_k \rangle$ a self-similar log-normal distribution is obtained

TABLE I. Trends in Latent Heats of Vaporization and Low-Frequency Electronic Dielectric Constants Useful for Estimating Kinetic and Localization Effects in Cluster Formation

element	L_V, eV/atom	ϵ_0	element	L_V, eV/atom	ϵ_0
Ar	0.065	1.6	Ge	4.1	16
He	0.001	1.1	Sn	3.3	24
Xe	0.14	2.1	Na	1.1	∞
C	6.2	5.7	K	0.9	∞
Si	4.2	12	Cs	0.75	∞

centered at $\langle n_k \rangle$. It should be noted that inert gas coagulation without significant evaporation may be more likely for large k for clusters with liquid-like or close-packed structures, because the heat of fusion should be related to the surface/volume ratio. For open or network structures such fusion may be sterically hindered unless local melting can occur at the intercluster fusion interface. Thus for nearly close-packed systems the sticking coefficient $f_{ij} \to 1$ with increasing i and j, but this may not be the case for open, network structures. For the latter τ may be too small for fusion to take place before rarefication freezes the cluster distribution at smaller values for large i and j.

C. Two-Component Condensation

In some experiments the sample is prepared as a homogeneous vapor which is condensed by adiabatic expansion. For these experiments the kinetic theory of section IIA should be adequate providing cluster stabilization by closed shell effects are neglected, i.e., providing f_{ij} = const. In other experiments the sample vapor is entrained by a carrier gas. The entrainment has two effects. The most important one is an expansion of the effective condensation regime, corresponding to larger values of $\langle n_k \rangle$ and the terminal time τ. This point has been demonstrated by Smalley and co-workers, who showed that with entrainment $\langle n_k \rangle$ (and similarly τ) could typically be increased by at least a factor of three.[2]

The second effect found in a two-component gas is a size-dependent change in the relative collision rates of sample clusters. If the boiling point of the carrier gas is much lower than that of the sample, during the condensation of the latter the former remains as monomers. Some typical heats of vaporization and boiling points are listed in Table I for convenient reference. When the carrier gas partial pressure is too high, collisions of sample clusters with the carrier gas followed by loss of the latter from the beam will cool the former so rapidly as to nullify the beneficial effects of inertial entrainment. The kinetics of an open system contain too many factors to specify all these competing effects in detail. In practice it seems likely that experimentalists will continue to be more likely to publish concentration spectra which exhibit larger values of $\langle n_k \rangle$.

D. Ionization Kinetics

Two steps in the formation of ionized n-atom microclusters are dinstinguishable: the condensation of neutral clusters, and the ionization of these neutral clusters. For some samples the ionization cross sections are expected to be relatively slowly varying functions of n, while for others this need not be the case. One should distinguish positive ions (electron removal) and negative ions (electron capture by neutral clusters from

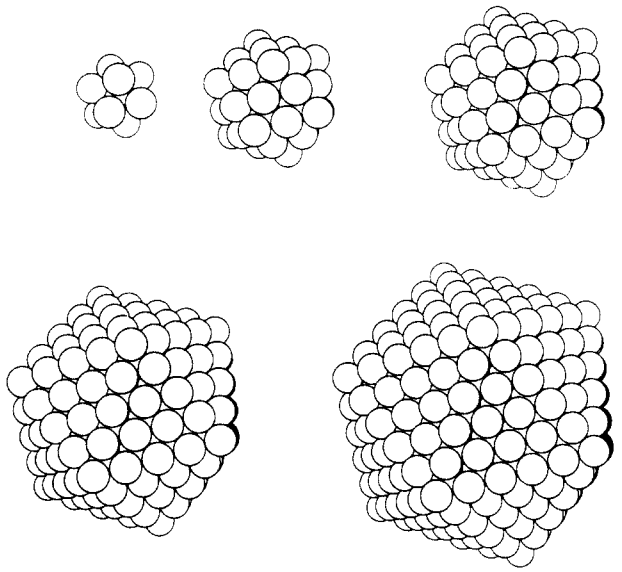

Figure 2. The first five Mackay icosahedra, corresponding to n = 13, 55, 147, 309, and 561, respectively. Reprinted with permission from ref 15. Copyright 1967 Elsevier, Amsterdam.

the plasma containing positive ions and electrons). One should also distinguish ions produced by multiphoton ionization which transfers energy of order 10–15 eV to the cluster, and electron beam ionization, where a large fraction of the electron beam energy (of order 30–50 eV) may be transferred to the cluster. In bulk solids electron beam excitation is dominated at high energies by collective plasma excitations[6] in multiples of $\hbar\omega_p$, where ω_p is the plasma energy and generally lies in the range of 15–30 eV. The excited plasma oscillation may then emit an ionized electron. It would appear in general that electron beam ionization would disturb the neutral cluster population more than photoionization, for example, by production of secondaries through fragmentation.

In most experiments ionization takes place following neutral cluster condensation. However, in the case of Ar (section IIIB) it was found that superior cluster spectra were obtained by ionizing monomers and condensing ionized clusters using the ionized monomers as seeds. Thus for Ar, ionization of large neutral clusters has a disruptive effect, producing large heating and probably substantial evaporation and fragmentation. The extent of these disruptive effects is expected to vary significantly with the type of chemical bonding and specific discussions will be given for each case (molecular, metallic, and network).

III. Inert Gas Clusters

Interatomic interactions between inert gas atoms involve a central pair force which is extremely well known and so this system is popular with theorists. The low melting and boiling points of inert gases as well as their low reactivity makes them equally attractive to experimentalists. Finally the simple central forces imply that the most stable clusters will be the ones with high density. These might correspond to the Mackay icosahedra[7] with spheroidal closed shells at n = 1, 13, 55, ..., $(1 + \sum(10p^2 + 2))$. The first five Mackay clusters are illustrated in Figure 2; note the pentagonal symmetry characteristic of an icosahedron. The interior atoms of these icosahedra are 12-fold coordinated, just

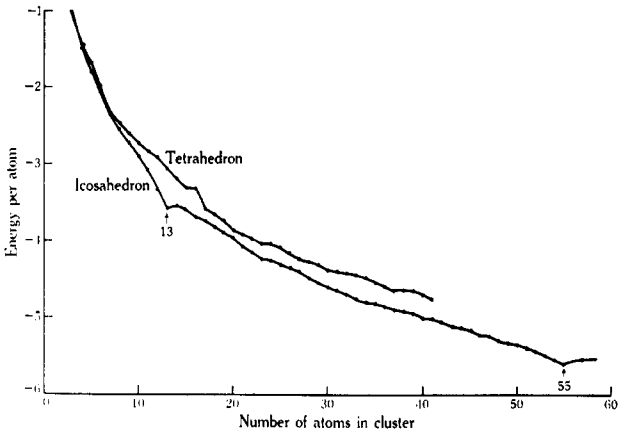

Figure 3. Comparison of cohesive energies of icosahedral and tetrahedral (close-packed) clusters as a function of n. Reprinted with permission from ref 8. Copyright 1970 Commonwealth Scientific and Industrial Research Organization, Melbourne, Australia.

as in a close-packed lattice. The 13-atom icosahedron is denser than the 13-atom cubo-octahedron which is the building block of close-packed crystals. The energy of icosahedral clusters calculated with a Mie potential is compared to clusters with local close-packing and tetrahedral morphology[8] in Figure 3. From this plot upper bounds on the local stabilization energies at n = 13 and n = 55 can be estimated, although since the clusters were not fully relaxed these values (for instance of dE/dn or d^2E/dn^2) may be too high by about a factor of 2.

The calculations shown in Figure 3 were extended to n = 2000 atoms with spacings $\Delta n/n \sim 0.3$ for $n > 50$. Up to n = 2000 the energy/atom of the icosahedral clusters remained ~2% lower than that of the close-packed clusters, but still ~6% higher than the bulk crystalline value. For n = 13 the icosahedral cluster has density ρ = 0.73 which decreases[7] to ρ = 0.69 with increasing n. The close-packed crystalline density is ρ = 0.74. Experiments on supported small metal particles[8] suggest that the cross-over between icosahedral and close packed energies may occur between $n = 10^5$ and 10^7. Because of the low temperatures of deposition in practice this cross-over may be kinetically rather than energetically determined.

A. Xe Clusters

The existence of magic numbers, i.e., maxima in concentration profiles c_n in cluster spectra, was convincingly demonstrated for Xe by Echt, Sattler, and Recknagel.[9] Their concentration profile, shown in Figure 4, exhibited Mackay icosahedral peaks at n = 13, 55, and 147, as well as a peak at n = 19 which could be ascribed to a double icosahedron.[10] Up to n = 40 sublimation energies $\Delta E_n = E_n - E_{n-1}$ were calculated for neutral clusters, with the results shown in Figure 5. These explain the peaks at n = 13 and 19, and together with the Mackay peaks at n = 55 and 147 make a convincing case for geometrical sphere-packing models of the structure of stable Xe clusters.

The n = 19 structure can also be described as an n = 13 icosahedron with a 6-atom cap from the p = 2 shell. The next cap may be either adjacent to the first cap and share two edge atoms, giving n = 23, or be antipodal, giving n = 25. Both n = 23 and n = 25 are

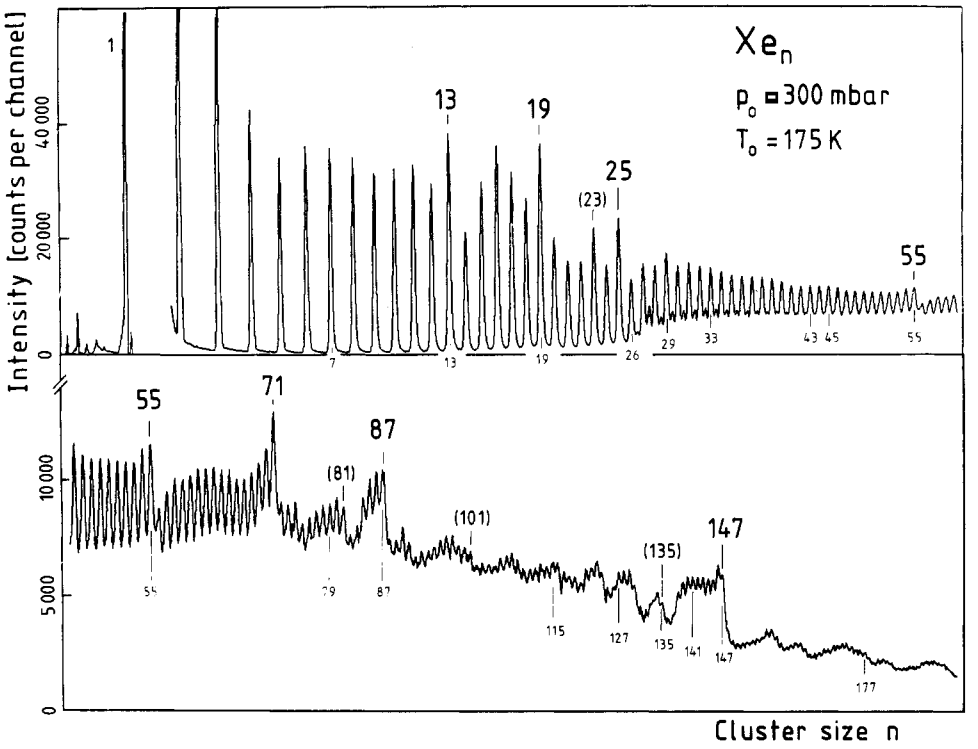

Figure 4. Concentration profile of Xe clusters produced by adiabatic expansion and ionized by an electron beam. Reprinted with permission from ref 9. Copyright 1981 American Institute of Physics.

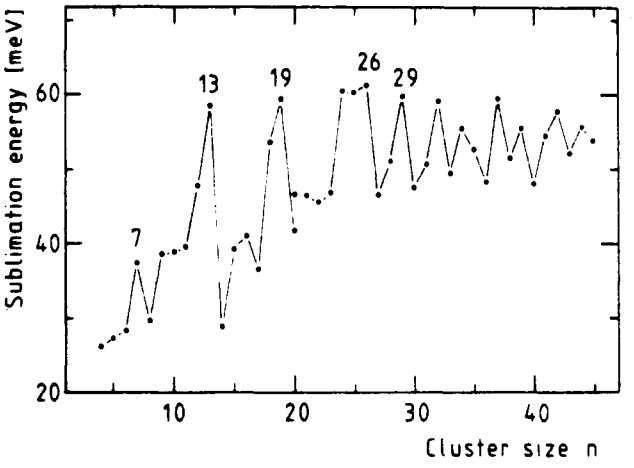

Figure 5. Sublimation energy $\Delta E_n = E_n - E_{n-1}$, calculated for Ar clusters. Figure reprinted with permission from ref 9. Copyright 1981 American Institute of Physics (E_n from ref 10).

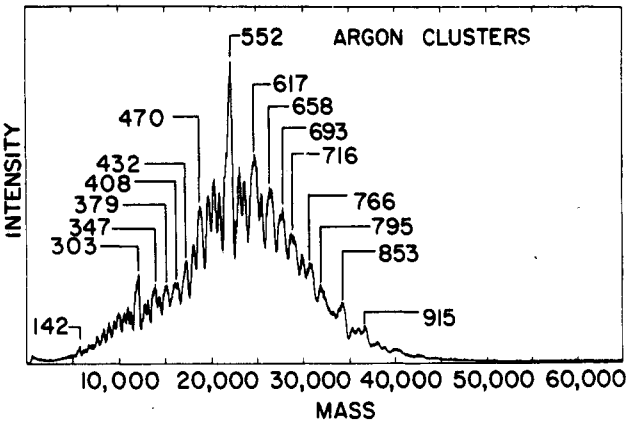

Figure 6. Large Ar_n^+ clusters grown from Ar^+ seeds gave this concentration spectrum.[12]

magic numbers in Figure 3, but $n = 25$ (antipodal caps) is stronger. This pattern is repeated for $p = 3$ with antipodal caps at $n = 87$, but there is no evidence for edge-sharing caps in the $p = 3$ shell of Xe.

B. Ar Clusters

The results for Xe_n^+ shown in Figure 4 appear quite simple by comparison with the results obtained for Ar_n^+ by various workers. A dip at $n = 20$ (corresponding to evaporation to $n = 19$, section IIIF) was observed with neutral clusters produced by expansion through a nozzle followed by ionization by electrons, but no other peaks were seen.[11] When weakly ionized Ar was present in 2% concentration in He gas, expansion produced very large clusters (average n near 500).[12] One of these very large cluster spectra is shown in Figure 6. It takes up where Figure 4 left off, with peaks near the Mackay numbers $n = 147$, 309, 561, and 923. (The experimental values are systematically low by 1–3%.) The successful growth of these large Ar clusters was apparently made possible by two factors, growth from an ionic seed, and cooling by collisions with evaporating He monomers.

When $10 \lesssim n \lesssim 100$ Ar_n^+ clusters were produced by supersonic expansion followed by ionization by electrons, peaks were found[13] at $n = 3$, 14, 16, 19, 21, 23, 27 in quite strong disagreement with the Xe_n^+ results shown in Figure 4. The origin of this difference became apparent when positive Ar^+ ions were seeded into Ar gas expanding through a nozzle.[14] Peaks at $n = 13$, 19, 55, and 71 were obtained, in general agreement with the results of Figure 3. Moreover, fine structure observed at $n = 19$, 23, 26, 29, 32, and 34 as well as at $n = 49$, 46, 43 was predicted for the $p = 2$ shell by a simple model. In this model the first set is formed by adding atoms in edge-sharing (5 + 1)-atom caps of a pentagonal ring of five face-centered atoms plus a vertex cap, which maximizes the number of bonds in a partially filled Mackay shell. (The double icosahedron at $n = 19$ is a special case of this construction, where one cap has been

added.) The second set is obtained by cap removal. The two procedures cross near $n = 39$, and no peak is found in the range $34 < n < 43$.

It is interesting to extend this analysis to the $p = 3$ shell ($55 < n < 147$) with peaks at $n = 71$, 87, 101, and 135 (see Figure 4). The first three peaks correspond to cap addition, the last to removal of all vertices, and the crossover region is $101 < n < 135$. The added caps are $10 + 5 + 1$ for the first two caps (antipodal, no edge-sharing) and $8 + 5 + 1$ (only one edge unavoidably shared). This construction is symmetrical for $n = 135$, but it has no symmetry for $n = 71$ and $n = 101$, and only axial symmetry for $n = 87$. This is surprising because many complex and symmetric clusters in the range $100 < n < 150$ with icosahedral symmetry have been constructed[15] which are not observed. One of these ($n = 115$) is derived from the $n = 55$ icosahedron by adding a shell of atoms at stacking fault positions. Because stacking fault energies are very small, it is indeed unexpected that capped structures with little or no symmetry are preferentially observed.

By restricting the range of models to those identified above for $p = 2$ and $p = 3$, we can analyze the data for $p = 5$ ($309 < n < 561$) shown in Figure 6. (There are no data at present for $p = 4$.) The $309 + \Delta n_+$ values are $\Delta n_+ = 44$, 32, 29, and 24. The experimental resolution in this high n range is probably ± 2 for Δn. The important point is that a cap will contain $15 + 10 + 5 + 1 = 31$ atoms and so $\Delta n_+ = 44$ cannot describe a simply capped 309-atom icosahedron. However, if we round this cap by adding to it the three atoms from each edge but not the corner atoms from the next row, we get $\Delta n = 46$, in agreement with the first Δn_+. Subsequent Δn_+ values look like simple caps, with increasing edge-sharing.

The $p = 6$ ($561 < n < 923$) data in Figure 6 follow a similar pattern for Δn_+. The basic cap contains 51 atoms, but $\Delta n_+ = 65$, 41, 35, 23. If we again round the basic cap by adding the edge but not the corner atoms from the next row, we get $\Delta n_+ = 71$. It seems that for large n capping is still the basic growth increment, but the cap edges are rounded because of relaxation of icosahedral strain (section IIID). Nevertheless these concentration peaks for large n are reproducible.[12]

The patterns for Δn_- for $p = 5$ and 6 ($\Delta n_- = 82$ and 62, respectively) correspond to that for $p = 3$, where $\Delta n_- = 12$ (removal of all vertices). This is the first stage of vertex rounding. For $p = 5$ and 6, if we remove each vertex atom and its five nearest neighbors, we would have $\Delta n_- = 72$. This is in reasonable agreement with experiment. Because of surface tension vertex rounding is plausible in larger clusters and it is often observed in supported microparticles.[15]

The chief conclusion to be drawn from these rather successful models is that starting from Ar^+ seeds in some sense stabilizes or directs cluster growth more effectively than producing Ar_n clusters by expansion and ionizing them subsequently. Specifically, growth from an ionic seed maximizes bond number most effectively. Four questions now arise: Why does Ar behave differently from Xe? Why does starting from an ionic seed not only stabilize $n = 55$ when direct condensation fails but also maximize bond number for $13 < n < 55$ ($p = 2$)? Why do the added caps want to share edges for $p = 2$ but do not want to share edges for $p = 3$? Why are capped structures observed instead of more symmetrical structures in the intermediate ranges between Mackay icosahedra?

TABLE II. Coordination Numbers Z of Cluster Sites for Close-Packed Tetrahedron and Mackay Icosahedron.

	face	edge	vertex	ad atom
tetrahedron	9	6	6	3
icosahedron	9	6	5	3

C. Dimerization and Charge Localization

One of the questions most often raised about cluster concentration profile peaks or magic numbers is what effects will be produced by differences in charge state (+/0/−) energies and/or kinetics. As we saw in sections IIIA and IIIB, such differences are observed experimentally and their weights are quite different for Ar_n^+ and Xe_n clusters. We know that forces between inert gas atoms can be scaled and that the law of corresponding states applies more accurately to monatomic inert gases than to any other physical system. What are some of the physical mechanisms responsible for the large chemical differences between Ar (+/0) and Xe (+/0) microcluster statistics?

The first step towards answering this question is the recognition[16] that ionization of an inert gas cluster may produce a dimer ion (DI). The heating associated with DI formation was found by a molecular dynamics simulation to accelerate monomer evaporation,[16] but the change in evaporation rates from Ar_n^+ to Xe_n^+ was small and scaled approximately with T_m, the bulk melting temperature. Ionization heating was shown to destabilize neutral clusters magic numbers on a scale of nanoseconds, suggesting that observed magic numbers represent stable ionic clusters grown after ionization occurred, rather than before. However, the kinetic effects associated with such evaporation, while substantial (section IIIF), appear insufficient to explain the chemical differences between $Ar^{(+/0)}$ and $Xe^{(+/0)}$ microcluster statistics.

Many atoms in microclusters are surface atoms, and in general the energy of a surface DI (both atoms are on the cluster surface) is reduced relative to a bulk or interior DI. This energy difference has not been measured directly, but something closely akin to it is known: this is the energy of a surface exciton (bound electron/hole pair) compared to a bulk exciton. Near the surface dielectric screening is much less effective than in the bulk, leading to greater charge localization and to a reductrion of surface exciton energy compared to bulk exciton energy. Because this shift depends on the dielectric constant ϵ and the electron and hole interatomic transfer integrals (conduction and valence band widths), this shift again does not scale from Ar to Xe. The experimental values[17] for the exciton shifts are $\alpha = 0.6$ eV for Ar ($\epsilon = 1.6$) and $\alpha = 0.1$ eV for Xe ($\epsilon = 2.1$). Most of this shift α arises from electron, rather than hole, localization. The hole localization energy β may be smaller than the electron localization energy by the ratio of conduction to valence band width, which may be a factor of 10 or more, and this factor may be about the same[18] for Ar and Xe.

In a simple model the ionic localization energy δE_{loc} and band width scale with $Z^{-1/2}$ where Z is the coordination number listed for various sites in Table II.

Ionization thus stabilizes edge, vertex, and ad atoms. More generally, the hole localizes on outermost sites. Thus in a cluster containing one cap the hole will localize on the vertex atom of that cap, but edge atom energies of the cap will also be lowered. This will tend to promote growth of adjacent caps. It is tempting to speculate that ionic localization explains why adjacent caps grow on Ar_n^+ clusters (section IIIB) but are much weaker for Xe_n clusters (section IIIA). In effect adatoms captured by an ionized cluster diffuse on its surface and finally preferentially stick at edge sites of caps rather than nucleate new caps.

We saw in connection with Figure 3 that icosahedral clusters are expected to be stable with respect to close-packed clusters with tetrahedral morphology for $n >> 1000$. Eventually a second layer may form on the same cap before the first layer is completed. Such runaway growth of a close-packed face might constitute a kinetic path for conversion of icosahedral to close-packed tetrahedral clusters. By attracting atoms to cap edges rather than to cap centers (which are favored by Van der Waals forces) the localized ionic charge acts to suppress this instability, which we expect will become important only for $n \sim 10^6$.

This is a convenient point to mention the results obtained in electron diffraction studies of Ar microclusters.[19] These showed microcrystalline patterns with $n \sim 500$. The clusters were prepared in a high-pressure neutral expansion quench and were not deliberately ionized. They were ostensibly homogeneously nucleated. It seems possible that the 50 kV electrons used for diffraction fragmented much larger clusters with $n \geq 10^6$ which were indeed crystalline for such large n values. It seems unlikely that clusters with $n \sim 500$ grew in the closer packed crystalline structure. The average cluster size is probably determined by average transit time through the 50 kV electron diffraction beam, which can damage clusters by evaporation and fragmentation. Both take place at a very high temperature and it is likely that the clusters so produced would have very rough (non-close-packed) surfaces. Such surface roughening could explain why several Bragg peak strengths (including the (111)) were anomalous.[19] Incidentally, the inhomogeneous strain generated by rough surfaces would broaden the Bragg peaks and cause n to appear to be much smaller than its true value, which could easily have been $>10^4$.

D. Strain

It was mentioned in section IIIB that for $n \sim 350$, cluster caps of Ar_n^+ appear to be rounded. This is a natural result of the icosahedral geometry, which makes lateral bond lengths $\sim 5\%$ greater than radial bond lengths.[7,15] Calculations of relaxed close-packed interplanar spacings show radial contractions of nearly 10% due to the internal pressure of outer layers on inner layers.[20] Similar lateral contractions near cap edges could be expected from edge rows. The two effects correspond to surface and edge tension, respectively.

Can strain relaxation (edge or corner rounding) explain the differences in magic numbers between Xe_n and Ar_n^+ clusters for $10 < n < 100$? The answer seems to be no, for two reasons. The edge-rounding effects are small for $n \sim 350$. Generally speaking, strain relaxation scales with some characteristic length (cluster or cap diameter) l like l^2, i.e., like $n^{2/3}$. In the range $10 < n < 100$ strain relaxation effects should be very small.

The second reason why strain relaxation must be irrelevant to the $Xe_n - Ar_n^+$ differences is that the ratio of the DI bond length d^+ to the dimer bond length d is $d^+/d = 0.66$ (Ar) and 0.75 (Xe).[16] If cap relaxation or contraction towards the cap center were important, the clusters with the larger contraction would be the ones with disjoint caps, i.e., Ar would have disjoint caps. However, the disjoint caps are actually found for $10 < n < 100$ in the Xe clusters.

Strain relaxation is a collective energetic effect, whereas individual site preference energies determine cluster structure by influencing the kinetics of monomer addition. This shows microscopically how the differences between Xe_n, Ar_n and Ar_n^+ magic numbers arise kinetically.

E. Branching Kinetics

The development of competing adjacent or antipodal capping patterns can be analyzed kinetically. Suppose we have two clusters. The first contains n_c atoms and is in equilibrium with a vapor of n_v atoms at pressure p_o. The second contains $n_c + \delta n$ atoms. The first may correspond to a Mackay cluster with two adjacent caps, the second to a cluster with two antipodal caps. In that case $\delta n = p$ and the question is whether we expect to observe both magic numbers or not. Fluctuations in competing growth channels occur on a scale of $n_c^{1/2}$. Thus so long as the condition $p = \delta n \ll n_c^{1/2}$, the answer would appear to be yes. In effect we assume that site-preference energies are less than condensation energies. The condition $p \ll n_c^{1/2}$ is reasonably well met for the case $p = 2$ ($n_c \sim 25$) and $n = 23, 25$ are observed for Xe_n clusters. For Ar_n^+ clusters only $n = 23$ is observed, hence it is possible that charge localization energies can increase site preference energies to make them comparable to condensation energies, at least for Ar.

F. Evaporation

Each observed cluster concentration peak or magic number arises from energetic stabilization with or without kinetic branching selection. The latter can be studied by comparing cluster statistics starting from charged or neutral seeds, while the former can be studied by comparing the annealing effects of cluster ionization by excluding dissociation products from the concentration profile measured by the detector after ionization.

Some recent results[21] for Xe_n^+ clusters with n near 55 (Mackay icosahedron) and 71 (same with one cap) are shown in Figure 7. With dissociation products removed c_n has been reduced by as much as 99% for $n = 57$ by monomer evaporation first to $n = 56$ and then to $n = 55$. The relative stability of $n = 58$ is that of a triad in the $p = 3$ shell outside the $n = 55$ closed shell. This increases up to a pentamer, the first closed ring which is centered on a vertex, at $n = 60$, for the longer delay time. The small peak at $n = 74$ starts a new cap which echoes the jump from $n = 57$ to $n = 58$.

By comparing the concentration profiles in Figure 7 we can see that monomer evaporation stimulated by ionization plays a decisive role in enhancing magic numbers in the spectra of clusters originally grown in

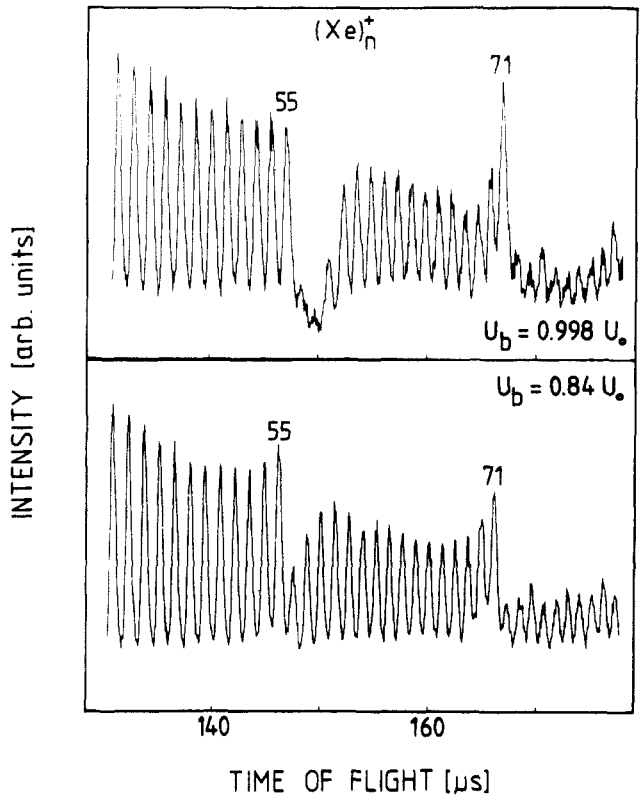

Figure 7. Effects of evaporation following electron beam ionization.[21]

the neutral state. Evaporation rates reflect changes in the total energy of the ionized cluster, which during evaporation may be at a higher temperature than the cluster grown from an ionized seed and cooled by expansion. The neutral cluster has also grown according to different branching kinetics. It is therefore expectable that the two kinds of concentration profile will in general exhibit differences in the way shells are filled.

The typical signature of profile refinement or annealing by evaporative enhancement—a peak at n, followed by a deep valley for $n + 1$, $n + 2$, ... until a stable unit or ring is formed in the next shell—is found not only in ionized Xe_n spectra, but also in Ar_n^+ spectra grown from an ionized seed.[14] Here evaporation is probably less important, but the dip at $n + 1$ is probably associated with the reduction in binding energy of the $(n + 1)$st atom because of charge localization. An interesting case is the peak at $n = 49$ followed by the dip at $n = 50$. For $n = 49$ the ionization charge will be uniformly distributed on the 10 atoms bordering the missing 6 cap atoms. At $n = 50$ the extra atom begins to fill in the last cap and, as it is the outermost atom, the ionization charge will be localized on it. This is energetically much less favorable than having the ionization charge spread over 10 atoms.

IV. Metallic Clusters

Our attention now shifts to metallic clusters. Rare gas clusters, although complex, benefit from the simplicity of interatomic forces which are central and predominantly two-body, as reflected by close-packed crystal structures. Many elemental metals are not close-packed, and their crystal structures can be understood qualitatively only from electronically mediated and quantum-mechanically determined collective interactions.[22] These are strongly influenced by the exclusion principle, whose consequences in real space for clusters of finite size are not easily visualized. Thus to the very large number of configurational possibilities already encountered for rare gas clusters we must now add in general the partially directional pair forces found with metallic binding.

Taken altogether, these new complexities render the problem of interpreting concentration spectra alone an imposing, if not impossible, task, for metallic clusters. Fortunately there are some simplifications in the metallic case. Magic numbers for metallic clusters in (+/0/−) charge states appear to be nearly the same.[23] The ionization charge in metallic clusters should be much less localized than in insulating clusters, so this conclusion is in agreement with theoretical expectations. Variations in other experimental parameters (even including ionizing electron beam energy E_i in the range $10 < E_i < 300$ eV, with fragmentation at $E_i > 20$ eV) also do not influence the observed magic numbers in Pb_n clusters.[23]

The elemental metallic families of common valence generally exhibit a variety of crystal structures. While Al is close-packed, Ga has a complex crystal structure. Similarly Pb is close-packed, but Sn has several partially covalent crystal structures with low coordination numbers. Only the alkali metals have the same crystal structure (body-centered cubic).

Efforts to produce large metallic clusters, similar to those discussed in section III for inert gases, were often unsuccessful. Large clusters Pb_n were obtained[23] by quenching in He (but not other inert gases). Large Na_n clusters ($n \leq 65$) were grown[24] from Na^+ seeds and cooled by Ne, Ar, and Kr (but not He, which gave $n \leq 20$). Unfortunately the concentration spectra so obtained seem to be distorted by measured masses which were 5% too low and by a high beam temperature.[25]

A. Alkali Metals

Electronic cohesion in the alkali metals was explained by Wigner and Seitz in terms of the nearly free electron model.[26] The electronic energy of crystalline alkali metals can be calculated almost as if the electrons were confined to a box. This suggests a spherical well (or "liquid drop") model for alkali metal clusters, a model defined by well depth and radius which is often solved in quantum-mechanical texts. The resulting energy levels form shells labelled by angular momentum l and principal quantum number n. This situation is reminiscent of the shell model for nuclear structure, where the energy levels are made more complicated by a strong spin-orbit interaction which is absent here. Thus the energy levels of alkali metal clusters may represent an ideally simplified analogue of nuclear shell structure.

The nearly free electron model for alkali metal crystals is extremely successful in practice. The energy splittings of the parabolic free electron states by Bragg diffraction from the crystal potentials associated with lattice planes have been measured in many experiments and are typically at least 10 times smaller than the band width occupied by one valence electron/atom. As a result the cohesion of alkali metal crystals does not arise from covalent bonds formed by single electron pairs (or even fractional or resonating electron pairs). Instead, as Wigner and Seitz showed[26] and has since been doc-

umented in many modern calculations,[22] alkali metal cohesion arises as a volume energy not expressible as a sum of two-body interactions. This volume energy arises primarily from exchange between electrons of parallel spin and dynamical correlation between electrons of anti-parallel spin. In effect the electron interactions with the alkali metal ions are just large enough that the latter can be regarded as a constant and uniform static background positive charge which cancels the average Coulomb repulsion between electrons. The absence of conventional chemical bonding or two-body interactions in alkali metals explains why these otherwise unpleasant materials have been studied so extensively by physicists.

The "liquid drop" or shell model of nuclei is based on a similarly simple model. Nuclei interact through a repulsive interaction which is strong but very short range and an attractive interaction which is weak but with a range much greater than the average internucleon spacing. As a result nuclear collapse is prevented mainly by the kinetic energy of the nucleons which obey Fermi statistics, just as for electrons in metals. Drops containing only a few nucleons can be anisotropic and the rotational kinetic energy of an anisotropic droplet can be important, as it removes degeneracies and can reverse energy level orderings. In nuclei where spin-orbit interactions are large, elaborate calculations have been carried out to combine these two effects, but in alkali metal clusters the absence of spin-orbit interactions may greatly simplify the calculations as well as reduce the number of adjustable parameters.

The nuclear shell or liquid drop model is known to be successful as soon as $n \gtrsim 10$ particles are involved. It is for this reason that we may expect that this abstract model, unfamiliar to many chemists, might provide a very successful description of the structure of alkali metal microclusters. Because the cluster cohesion is a volume property, and not describable in terms of pairwise interactions, one can discard the complexity of an explicit discrete spatial model in favor of a more continuous or liquid-like description that explains all the main features of the experimental data. One can go further and say that it is difficult to imagine an experiment which would be sensitive to the discrete structure of an alkali metal microcluster.

Several chemists have mentioned to me that they find this "jellium" or droplet model of alkali metal microclusters difficult to understand. I believe the mental block here is primarily the result of the way that quantum chemistry is ordinarily presented in terms of overlapping atomic orbitals normally occupied by pairs of electrons to form single bonds. This approach is appropriate to covalently bonded molecules or solids, but it is not a useful description for metals.[22] However, the question continues to arise and the reader who feels that alkali metal clusters "ought" to have polyhedral structures is directed to a recent note which shows that this is not the case.[22]

A very accurate concentration spectrum for Na vapor quenched in 6 atm of Ar gas through a small nozzle was obtained by Knight and co-workers,[27] as shown in Figure 8(b). The spherical magic numbers n = 8, 20, 40, and 58 associated with closing the 1p, 2s, 2p, and 1g shells are unambiguous. (Chemists accustomed to (nlm) symbols for atomic orbitals may be surprised to see 1p and 1g levels. The rule $n \geq l$ applies to Coulomb potentials but not to well potentials.) A weaker peak at n = 18 in Na_n clusters associated with closing the 1d shell is enhanced in K_n clusters,[28] in accordance with theoretical calculations.[29]

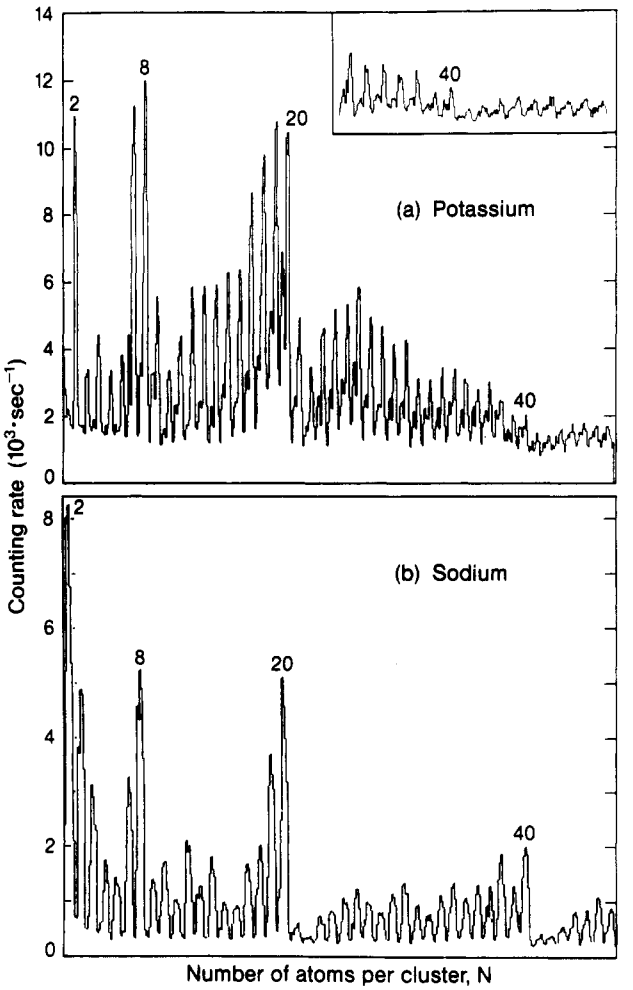

Figure 8. Concentration spectra of K and Na vapor adiabatically condensed in Ar.[25,27]

Perhaps the most remarkable feature of the alkali metal spectra is the almost quantitative correspondence between c_n and $g(n)\,h(n)$, where $g(n) = 2E(n) - E(n-1) - E(n+1)$, i.e., the electronic second energy difference. (Here $h(n)$ is a smooth function describing coagulation kinetics of the type shown in Figure 1.) Note the pronounced dips in c_n following the spherical magic numbers. These are present in the neutral cluster concentration spectra prior to ionization, since the peak for n occurs at n rather than $n + 1$. Presumably the additional binding energy $E(n+1) - E(n)$ gained by adding one atom outside a closed shell is small. Thus the corresponding sticking coefficient for monomer addition to a closed shell cluster is small.

A great deal of fine structure is apparent in the alkali metal spectra between the spherical magic numbers. In terms of the liquid drop model the obvious explanation for this fine structure is that spherical clusters are deformed to uniaxial ellipsoidal clusters to remove the degeneracy associated with the electronic m_l azimuthal quantum number. The total energy now contains the rotational kinetic energy of the ellipsoidal well in addition to the single-particle electronic energies.[30] (Readers not familiar with nuclear structure theory may wish to know that ellipsoidal droplets have been gen-

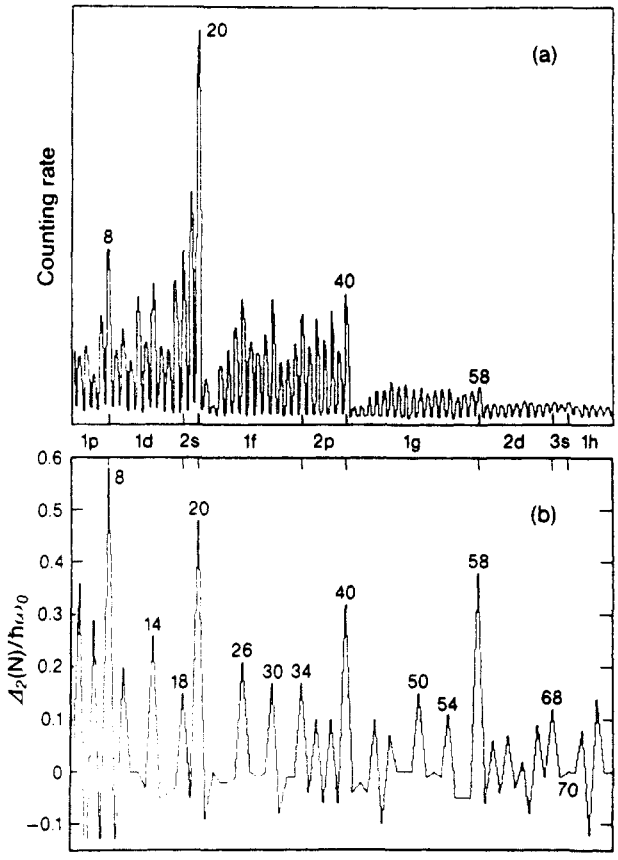

Figure 9. Ellipsoidal nuclear shell model calculations (b) of stability of Na clusters (a). Reprinted with permission from ref 30. Copyright 1985 American Institute of Physics.

erally accepted in that field for 50 years.) In Figure 9 (a and b) the results of this approach, analogous to the nuclear shell model, are compared to the experimental spectrum for Na, again in terms of $g(n) = \Delta_2(N)$, normalized against the rotational kinetic energy spacing $\hbar\omega_0$. The lifting of the subshell degeneracies explains peaks at n = 14, 26, 30 and so on, without containing *any* adjustable parameters.

An interesting feature of the ellipsoidal shell model[30] is that there is a quantitative difference in the magnitude of the energy difference $\Delta_1(E) = E(N + 1) - E(N)$ for ellipsoidal shells compared to spherical closed shells. For the spherical shells $\Delta_1(E)$ is typically three times larger than $\Delta_1(E)$ for the ellipsoidal shells. This means that the stabilization energy for the $(N + 1)$st shell is small for spherical N-shells, and hence the monomer sticking coefficient is reduced. For the ellipsoidal shells the stabilization energy is larger and the sticking coefficient is closer to unity. Thus c_{N+1}, c_{N+2}, and so on may be small even without evaporation for spherical N shells but not for ellipsoidal shells, as can be seen in Figure 9(a) for the spherical shells (N = 20, 40) and the ellipsoidal shells (n = 14, 16, 30, ...).

The experimental and theoretical alkali metal relative abundance spectra shown in Figure 9 illustrate an analytical point of general importance. Granted that the theoretical spectrum is in excellent agreement with the experimental spectrum, both as regards principal magic numbers (for example, n = 20, 40) and secondary magic numbers (n = 26, 30, 34), what does this really prove? After all, concentration spectra are one-dimensional and the actual clusters are three-dimensional. Don't we have to have three-dimensional diffraction data to establish three-dimensional structures? Is the liquid drop model merely an accidental success, and couldn't a polyhedral model work just as well?

These doubts can be answered in two ways. First we may consider a specific polyhedral model and show that it fails, as has already been done for alkali metal clusters.[22] However, this approach is a little too narrow, because one can always argue that some other polyhedral model might succeed.

The second answer to these doubts is much more general and is based on the concepts of information theory. For any one cluster size n the relative abundance spectra c_n and $c_{n\pm1}$ do not contain enough information to determine a three-dimensional cluster structure. However, Figure 9 contains values of c_n for $8 \leq n \leq 58$ which are very well fitted by theory. Let us say that each experimental c_n can be classified as strong, medium, or weak. The number of possible combinations of 50 numbers which can be three-valued is $3^{50} = 10^{24}$, which is astronomically large: the age of the universe in seconds is about 10^{16}. The chance that theory can assign the correct three values to the entire *set* of $\{c_n\}$ *by accident* is negligibly small.

I have discussed this case in detail because the excellence of the experimental and theoretical spectra in Figures 8 and 9 leave no doubt about the uniqueness of the result, yet many chemists continue to question both the theory and the experiment. It is difficult not to suspect that these doubts arise from unfamiliarity which is interdisciplinary in origin. In this respect microcluster science may perform a valuable service by reminding even experienced senior scientists of the importance of alternative view points.

B. Polyvalent Main Group Metals

Mass spectra have been reported[31] for In, Pb, Sb, and Bi. The In spectra are relatively featureless, and the Sb and Bi spectra are dominated by tetramers (the familiar 3-fold coordinated tetrahedra appropriate to trivalent anions). The interesting spectrum is the Pb spectrum[31] shown in Figure 10. The magic numbers are at n = 7, 10, 13 (note that c_{14} is very small), 17 and 19.

Crystalline Pb is close-packed, like the inert gases. One might expect Pb clusters to exhibit structures similar to inert gas clusters, i.e., the cluster structure might be explicable in terms of dense sphere packing (section III). This explains n = 7 (pentagonal bipyramid), n = 13 (icosahedron), and n = 19 (capped icosahedron). However, n = 10 and 17 are left unexplained by atomic packing.

A Pb_n cluster contains $m = 4n$ electrons, so that n = 10 (17) corresponds (according to Figure 8(b)) to filling the m = 40, 2p (68, 2d) spherical electronic shells. The m = 20 electronic shell corresponds to n = 5 atoms, too few to be approximated by a spherical well. The electronic 1g shell closed at m = 58 is not divisible by 4. We expect c_{14} to be small because it is 14 = (icosahedral 13) + 1. However, $c_{15} > c_{16} \gg c_{14}$, so that the n = 15 cluster may be stabilized by electronic shell effects associated with closing the 1g shell.

We therefore see that because of electronic effects "solid" structures (dictated by atomic packing) and "liquid" structures (determined by electronic shell effects) can alternate for $10 \leq n \leq 20$. This means that

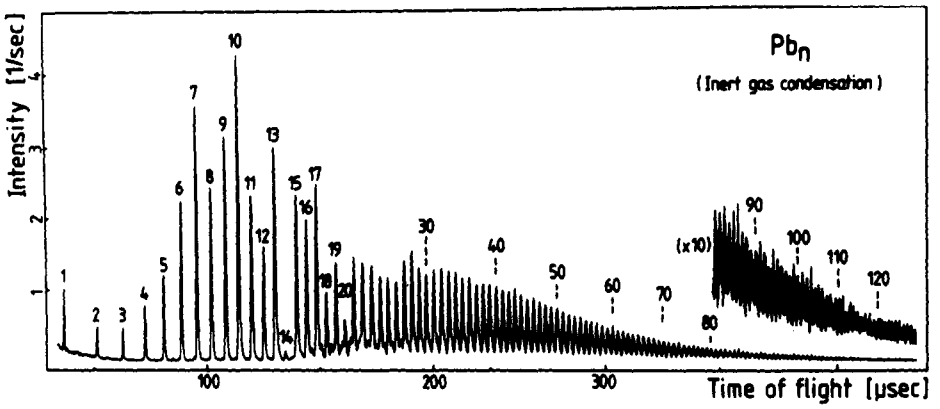

Figure 10. Concentration profile of Pb_n^+ clusters prepared by adiabatic expansion and electron beam ionization.[30]

for metallic cluster sizes on this scale the distinction between solid and liquid structures cannot be made from concentration spectra alone. While it may still be appropriate to speak of an effective monotonic cluster temperature T^* (defined in terms of vibrational energies), it is meaningless to speak of a smooth monotonic function of n which describes cluster melting at $T^*(n) = T_m^*(n)$. We can define $T_m^*(n)$ only for very large values of n (probably $\gtrsim 100$) where electronic shell effects are relatively small (correspondence principle limit).

Some recent results[23] for Sb clusters should be mentioned here briefly. Monomers readily aggregate to form Sb_4 clusters, so that the observation of magic numbers at $n = 4m$ was not surprising.[31] Recently such clusters have been doped with Ag and Pb with interesting systematic results.[23] These lead to a structural model of the Sb clusters as essentially bilayer crystalline fragments. Apparently Ag intercalates between these layers while Pb caps them. This is not surprising, in view of the remarkable behavior of Ag^+ ions in superionic conductors, as well as the large size of Pb. Oscillations in intercalativity of Ag as a function of m can be explained in terms of simple Sb bilayers at $n = 12$, 20, 28, ... and tetrahedrally capped bilayers at 16, 24, ...

The Sb coordination numbers in these bilayers are low (2- and 3-fold) and it is unlikely that these structures are energetically the lowest. However, they are very easily constructed kinetically using tetramer building blocks which can readily form rings and ring segments. Many of these features of Sb bilayers are similar to those of some models which have been proposed for network clusters which are discussed in section V. Thus the usual crystalline description of As, Sb, and Bi as semi-metallic may apply to these elements in microclusters as well.

C. Transition Metals

We have seen that two factors, atomic sphere dense packing and nearly free electron shell formation, may contribute to producing magic numbers in alkali metal and Pb spectra. Neither of these factors is expected to be effective for transition metal clusters. The d electrons in solid transition metals form energy bands separate and distinct from the energy bands of s–p electrons. Thus electron counting based on lumping together the s, p, and d electrons is not reliable and simple electronic shell effects of the nearly free electron kind are not expected for transition metals. On the other hand, we know from ligand field coordination chemistry that strongly directional, partially covalent bonds are a characteristic feature of partially filled d levels. This means that dense sphere packing based on simple central pair forces also should not occur for transition metal clusters.

Both these expectations are borne out by transition metal cluster concentration spectra obtained by rapid quenching. If this were the only result, this section would end here or perhaps not be included at all. However, the partially covalent nature of partially filled d levels has a silver lining, namely transition metals are well known for their catalytic activity, especially in the simplest case of chemisorptive hydrogen dissociation. Studies of reactions involving chemisorptive hydrogen dissociation on transition metal bulk surfaces have shown[32] that such reactions are extremely sensitive to surface orientation and especially surface roughness (e.g., surface steps). We may hope that chemisorptive hydrogen dissociation will be sensitive to transition metal cluster morphology, even if the transition metal binding energy varies so smoothly as not to produce magic numbers in the non-hydrogenated cluster concentration spectra.

The critical step in hydrogenation is dissociation of H_2. This has been demonstrated[33] for Fe_n clusters by measuring ionization potentials as a function of n for $9 \leq n \leq 25$. Overlapping the Fe gas pulse with a D_2:He gas pulse produced selective cluster deuteration. The extent of deuteration depends on the degree of overlap, and this can be used to define relative reactivity as a function of n. In Figure 11 both electron binding energy and relative deuterium chemisorptive dissociative reactivity are plotted as a function of n for Fe_n clusters.[33] For $n \geq 9$ an excellent correlation is obtained, showing that charge transfer from the metal complex is necessary for deuterium dissociation.

The ordinate scales of Figure 11 can be related by Boltzmann factors with an effective temperature T^* and a conversion factor ϵ

$$k_n/k_{n'} = \exp[\epsilon(I_{n'}-I_n)/k_B T^*]$$

where ϵ^{-1} is the ratio of electron binding energy differences to reaction-barrier differences, and $\epsilon = 1$ in a simple charge-transfer model. For T^* one should use a temperature intermediate between the reactor gas temperature, $T^* = 300$ K, and the boiling point of Fe, $T_b = 3000$ K, thus $T^* \sim 1500$ K. This is indeed con-

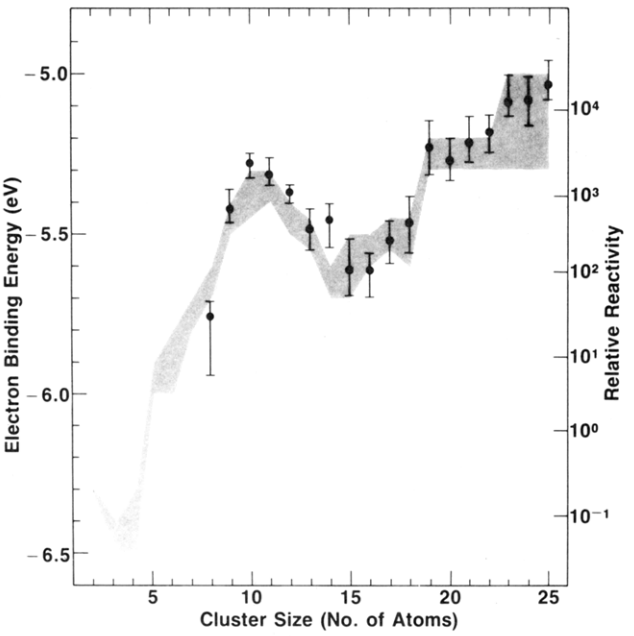

Figure 11. Comparison of electron-binding energy and relative deuterium chemisorptive dissociative reactivity for Fe_n^+ clusters.[32]

sistent with $\epsilon = 1$, and it suggests that deuteration requires hot metal clusters. This is consistent with the experimental finding[33] that a D_2:He ratio greater than 1:10 was needed for n-dependent deuteration.

The oscillations in electron binding energy shown in Figure 11 probably result from an interplay between structural and magnetic factors. In this respect Fe is by far the most complex case, because it is the most magnetic of the transition metals. The simpler cases of Nb_n and Co_n clusters exhibit relative reactivity oscillations which are very sharp,[34] as shown in Figure 11. Here we may hope that structural factors dominate because bulk Nb is nonmagnetic and bulk Co is much less magnetic than Fe. Also the crystal structures of Co and Nb are relatively simple (close-packed and bcc, respectively) compared to most polyvalent nontransition metals.

The striking feature of the Co data in Figure 12 is the well-defined abrupt increase in reactivity between $n = 9$ and $n = 10$. If the electron binding energy were simply decreasing smoothly with increasing n, such an abrupt decrease would not be expected. Similarly with Nb there is a well-defined nonreactive interval $8 \leq n \leq 12$, with $n = 8$ and 10 being especially nonreactive. At $n = 16$ an isolated nonreactive cluster is formed. Again there must be large oscillations in the electron binding energy or some spatial factor must be inhibiting reactivity. The Nb data in particular suggest some nonreactive shell structures, especially at $n = 8$, 10, and 16.

One possible explanation for this behavior is that the nonreactive clusters correspond to relatively open structures stabilized by the directional d–d bonds. Planar (110) faces of crystalline (bcc) W are not close-packed (because of the bcc crystal structure) and dissociative H_2 chemisorption does not occur on these faces,[32] although it does occur on rough W surfaces where more closely spaced W atoms may be found near steps. Also more open structures may have narrower d levels, which would increase electron binding energy for the nearly filled d^9 Co energy levels. For small n

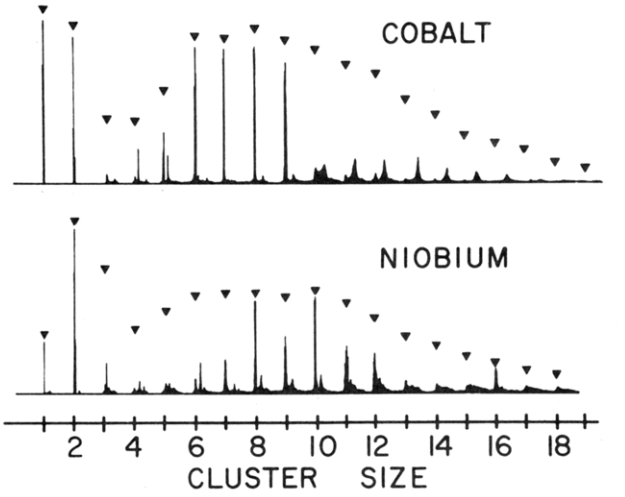

Figure 12. Relative deuterium chemisorptive dissociative reactivity for Nb_n^+ and Co_n^+ clusters.[33]

atom-centered structures are more open than structures based on tetrahedral or octahedral seeds (which grow into icosahedra and cubooctahedra at $n = 13$). A symmetrical atom-centered cluster at $n = 9$ has eight (111) neighbors which are not nearest neighbors of each other. For $n > 9$ some of the surface atoms of the cluster become nearest neighbors, and this might facilitate H_2 or D_2 dissociative chemisorption.

For the Nb clusters the d^4 configuration suggests that layered clusters might be stabilized, because in a layer structure the d levels split into σ, π, and δ components with degeneracies (including spin) of 2, 4, and 4. Thus the δ level would be filled at d^4, and bilayer structures could explain the exceptional nonreactivity of Nb_n for $8 \leq n \leq 12$. Especially at $n = 8$ and $n = 10$ the layers could be (4, 4) or (1, 3, 3, 1)—a double tetrahedron—or (5, 5) or (1, 4, 4, 1)—a double-square pyramid. (The bilayer polygons would be staggered.) This model could also explain the remarkable $n = 16$ isolated nonreactive cluster, as a (6, 6, 3, 1) tetrahedrally capped staggered hexagonal bilayer. All these clusters are stabilized by the π–δ energy gap characteristic of the d^4 configuration of Nb.

Heuristic models such as the foregoing are merely an indication of the direction large-scale quantum calculations may go in analyzing data such as that shown in Figure 12. The enumeration of all possible stable clusters rapidly becomes impossible, however, even for inert gas clusters,[15] for $n > 13$, so some suggestions based on chemical bonding considerations are likely to prove helpful for most elements.

V. Network Clusters

We have seen in section III that the dominant factor in determining inert gas cluster structure is dense sphere packing. In section IV the electronic shell energy of nearly free electrons stabilized clusters as spherical or ellipsoidal droplets. When we come to the network-forming elements from column IV of the periodic table, we expect covalent bonding to be the dominant factor leading to network formation, as in crystals. However, we know that most of the atoms in microclusters are at surface sites and have dangling bonds. These bonds may reform or reconstruct, as is known to be the case for the surfaces of crystalline diamond, Si,

and Ge. How important can we expect this reconstruction to be? We discuss this question first, and then review recent experimental data on C, Si, and Ge clusters.

A. Dense vs. Open Packing: Clusters vs. Crystals

The evolution of stable and metastable sphere packings starting from tetrahedral and octahedral seeds has been analyzed[10] in considerable detail up to $n = 14$. The tetrahedral seeds ($n = 4$) evolve first to the stable pentagonal bipyramid ($n = 7$, Pb_7^+) and thence to the icosahedron ($n = 13$, Xe_{13}^+, Ar_{13}^+, Pb_{13}^+). The octahedral seeds ($n = 6$) evolve to the second shell, $n = 14$ (6 (100) + 8 (111)), with a shallow minimum at $n = 12$.

When hard-sphere or Lennard-Jones potentials are replaced by covalent forces, the latter will be designed to favor certain bond angles, e.g., sp^3 bonds with 110° bond angles. The bond angles associated with tetrahedral and octahedral seeds are 60° and 90°, respectively. Central forces favor dense packing and 60° bond angles, so for these forces clusters generated by tetrahedral seeds are systematically lower in energy than those generated by octahedral seeds[8,15] up to large n. A covalent force field favoring 110° bond angles reverses this ordering[35] and favors octahedral structures topologically similar to those obtained with central forces for $6 \leq n \leq 9$. However, at $n = 10$ a stable minimum (6 (100) + 4 (111)) is found which has the topology of the carbon framework of adamantane, $C_{10}H_{16}$. This cage is the first symmetrical fragment of the diamond crystal structure. Because of the dangling bonds, the tetrahedral caps relax from the adamantane cage. It is this distortion that stabilizes $n = 10$. When the (111) shell is complete, at $n = 14$, large relaxation does not occur and $n = 14$ is not especially stable.

This auf bau description explains some of the reasons why we expect crystalline topology to persist in network clusters in the presence of dangling bonds; the latter generate relaxation effects which tend to sphericalize the cage without inhibiting further network growth. There are some other interesting electronic effects connected with dangling bonds. In the absence of relaxation the dangling bonds have a small energy gap and high electronic polarizability. Relaxation increases bonding which increases the energy gap and reduces the polarizability.

Because of surface reconstruction an overall trend in clusters towards more dense structures relative to their crystalline counterparts is expected. For Si, this trend should become more apparent for $n \geq 10$ with the first cage fragment of the diamond structure. For Sb the crystalline topology appears as bilayer hexagonal rings ($n = 12$).[23] An interesting case, which has not been reported experimentally at this writing, is Sn. The crystal forms with diamond (grey) and metallic (white) structures. Clusters could form with magic numbers at $n = 10$, 16 (diamond fragments) or $n = 10$, 13 (as in Pb). More dense structures ($n = 10$, 13) are expected according to the present discussion if energetic stability is the primary factor. However, kinetic factors may stabilize more open structures, so that measurement of the Sn spectrum is of great interest. Preliminary results[34a] on Sn suggest that $n = 10$ and 13 are magic numbers, so that our expectations that Sn microcluster structures more closely resemble those of Pb than those of Ge seem to be correct.

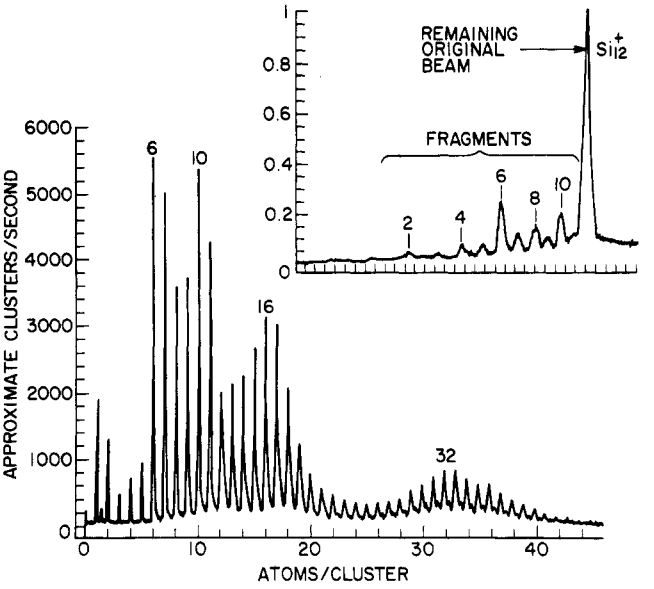

Figure 13. Concentration spectrum for Si_n^+ clusters and fragmentation spectrum for Si_{12}^+ (example). Reprinted with permission from ref 36. Copyright 1985 American Institute of Physics.

B. Silicon and Germanium

Among the network-forming elements Si may be the simplest because (unlike C) it has little propensity to form π or multiple bonds, and its tendency to form fractional bonds and increase its coordination number from four to six in the solid is much less than Ge or Sn. Thus for sufficiently large n we expect microclusters to assume a network structure similar to crystalline Si with tetrahedral sp^3 bonds internally and dangling or reconstructed bonds externally. On the other hand, we know that equilibration of network-forming materials (such as network glasses) can take place up to 10^{10} times more slowly than materials which form dense structures (such as metallic glasses). We expect drastic changes in the relative importance of monomer addition compared to fusion (section IIB) in network materials compared to materials with dense structures. Kinetically these differences would make their appearance in terms of anomalies in sticking coefficients as functions of cluster size n, and also cluster structure, which we hope to infer by separating kinetic and equilibrium effects on the concentration profile c_n. In more conventional chemical reactivity language, we expect the oscillations in reactivity barriers to be larger for network than transition metal clusters (Figure 11). These oscillations may also correlate less well with ionization potentials in network than in transition metal clusters.

Cluster spectra for Si_n^+ were reported with laser flash evaporation and supersonic carrier gas quenching.[36] A special feature of these experiments was the selective laser fragmentation and analysis of specific clusters. Thus the fragmentation spectrum of Si_{12}^+ is shown in Figure 13 as an inset together with the overall concentration spectrum. The branching ratios of fragmentation in Si_n^+ clusters for $2 \leq n \leq 12$ were measured.

A number of new features emerged in these concentration profile and fragmentation spectra. Although there are peaks in c_n at $n = 6$ and $n = 10$, there are no deep minima at c_{n+1}. Laser ionization does not produce

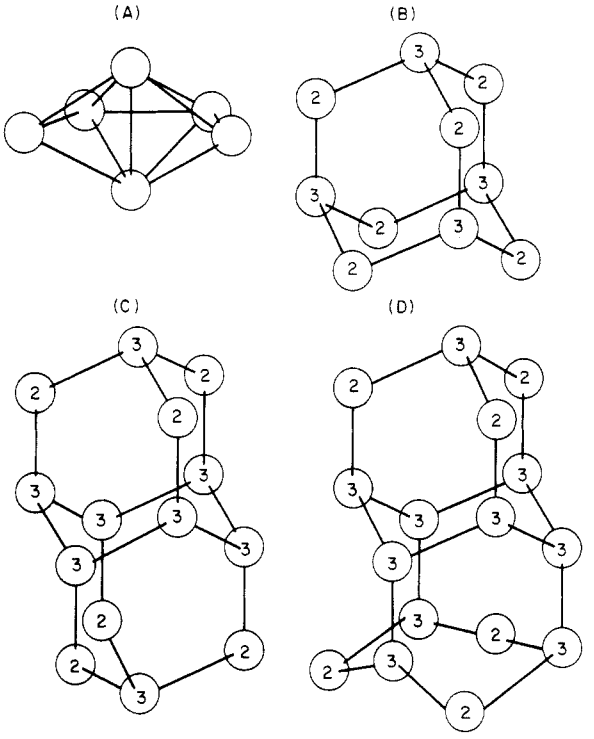

Figure 14. Possible crystalline fragments corresponding to Si_n^+ with n = 10, 14, and 16, as well as an octahedral (non-crystalline cluster) at n = 6. Reprinted with permission from ref 38. Copyright 1982 American Institute of Physics.

significant annealing (in contrast to inert gas clusters, section IIF), and the binding energy of a monomer to an $(n-1)$st cluster is not several times larger than the binding energy of a monomer to a magic-number-n cluster (as in the alkali metals, section IVA). Monomers also do not play an important role in the fragmentation spectra. Instead for photofragmentation the larger clusters ($10 < n < 12$) tend to cleave into clusters of nearly equal n. (From the statistical point of view, this means that bonding electrons are strongly influenced[37] by the exclusion principle, a conclusion scarcely surprising in the light of quantum chemistry.) These features in the oscillations of c_n in Si clusters are reminiscent of the oscillations in c_n for Fe_n^+ clusters (Figure 11).

A striking feature of the Si_n^+ concentration spectra is peaks in c_n at n = 16 and n = 32. These peaks provide strong support[38] for the structural models for n = 6 and n = 10. The n = 6 peak is an octahedral seed, while the n = 10 peak has the adamantane [6 (100) + 4 (111)] topology. Thus the tetrahedral crystalline topology first makes its appearance at n = 10, as distinguished from the merely cubic topology of n = 6. These two structures are shown in Figures A and B in Figure 14.

One can now place tetrahedral or hexagonal caps on the n = 10 cluster to obtain n = 14 or n = 16. It seems likely that both these structures, which correspond to sp^3 bonding and crystalline fragments (including possibly stacking faults, which have very low energy) are energetically stable. However, only the n = 16 peak is a maximum in the concentration c_n. Moreover, a similar maximum in c_n is seen at n = 32, with satellites at 32 ± 1, ± 2, which echo the 16 ± 1 pattern. The natural interpretation of these data is that they result from cluster fusion with no evaporation.[38] This result can be explained by assuming that cluster relaxation takes place slowly and that most of the heat of cluster fusion is removed by the carrier gas. By contrast, alkali metal clusters have liquid-like structures (section IVA), promoting rapid relaxation and elimination of the heat of cluster fusion by monomer metal evaporation. Apparently transition metal clusters also relax slowly, because there also experiment gives little indication of monomer evaporation.

The foregoing argument satisfactorily explains the kinetic origin of the peaks in c_n at n = 16 and 32 in addition to the energetically favored peaks at n = 6 and 10. It is incomplete, however, because by the same argument peaks at n = 20 and 26 should appear which are much stronger than the peak at n = 32. In Figure 13 this is definitely not the case. A possible explanation for the absence of peaks at n = 20 and 26 is that such peaks would be generated by the fusion reactions 10 + 10 → 20 and 10 + 16 → 26. Both of these reactions involve the n = 10 cluster, which may be especially nonreactive. Recent calculations[35] show a very large relaxation energy (~ 9 eV) for this cluster relative to an initial structure with equal bond lengths. The distances from the center of the cluster of the [(100),(111)] atoms relax from [2.7,1.9] to [1.8,2.8] in Å. The two subshells of the cluster have radially inverted. This large relaxation can be viewed as a consequence of dangling bond reconstruction, which is especially large because the average number of bonds in the adamantane cage is 2.4, which barely stabilizes the structure[38] in the absence of dangling bond interactions. Corresponding to this large relaxation energy we may expect a large reaction barrier. This argument does not apply to the reaction 6 + 10 → 16 because the n = 6 cluster is unstable against shear and so can easily react with n = 10 to form the structure shown in Figure 14D.

A test of the notion that mechanical stability can be used to connect relaxation energies to barrier heights is provided by the concentration spectrum of Ge. This spectrum[36] is quite similar to the Si spectrum, except that it contains weak peaks at n = 20 and 26. Crystalline Ge is well known[39] to be less stable mechanically than crystalline Si, both with regard to short-wavelength shear modes and to the transition pressure P_t required to transform to a metallic structure (similar to the transition state for cluster fusion). Thus we expect a smaller relaxation energy and a small barrier height for n = 10 clusters, which allows the n = 20 and n = 26 peaks to appear.

There is a general feature of the formation of network clusters which is observed with the Smalley synchronized supersonic and laser evaporative pulse technique which is not observed with more densely packed metallic or insulating clusters. Very small (and in practice so far uncontrollable) differences in the entrainment of the network clusters by the carrier gas can lead to large differences in the observed value of $\bar{n}$ (the average cluster size) for a given pulse. I believe that the origin of these differences lies in the large barriers to configurational rearrangement which are observed in many network materials and which are characteristic of their tendency to form amorphous or glassy solids.[38] For both Si_n^+ and Ge_n^+ clusters the spectra change dramatically in both mechanical stability (against ionization fragmentation) and kinetic yields near n = 10, as predicted

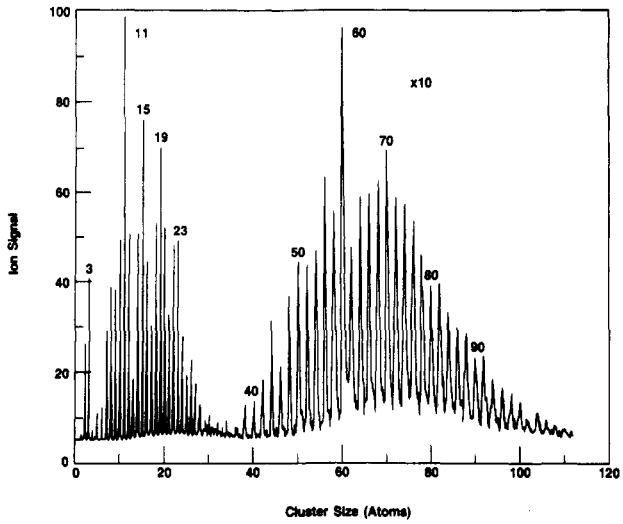

Figure 15. Concentration spectrum for C_n^+ quenched by adiabatic expansion in a carrier gas pulse and ionized to minimize photofragmentation for $n \geq 10$. Reprinted with permission from ref 42. Copyright 1984 American Institute of Physics.

by general network bond models.[38]

C. Carbon

The possibilities for reconstruction or rebonding of a network cluster increase enormously for carbon clusters, where multiple bonding stabilizes low-dimensional structures (such as chains and rings) relative to higher dimensional structures (graphite and diamond bulk phases). A classic discussion of this problem was given long ago.[40] For $n \lesssim 6$, C_n clusters are enthalpically stable as chains, whereas for $n \gtrsim 6$ monocyclic rings are favored. For very large n polycyclic structures are eventually favored; as yet there are not theoretical estimates of the n crossover value. The vibrational entropy of the chain is much greater than the ring, and at $T = 4000$ K (the boiling point of graphite) the chain-ring free-energy crossover was estimated[40] to shift to near $n = 10$. The signature of neutral chains (rings) is an oscillation of the double-bonded electronic energy with period $\Delta n = 2$ (4).

Concentration spectra for $C_n^{\pm}$ microclusters have been reported by several groups under a wide range of experimental conditions.[41-43] As might be expected, because of the low dimensionality of chains and rings the spectra depend quite sensitively on a variety of kinetic effects, such as multiphoton fragmentation. It is helpful to consider the spectra in three ranges, $1 < n \leq 10$, $10 \leq n \leq 30$, and $n \geq 30$. A "good" spectrum may be one that peaks near the middle of a given range. (Even this feature is sensitive to detection efficiency.) For example, a spectrum which shows large values of c_n in the range $10 \leq n \leq 30$ may describe c_n well in this range without fragmentation products. However, if many clusters are formed in this range, the values of c_n in the range $1 \leq n \leq 10$ may reflect not the initial cluster spectra formed as a result of quenching (which is largely exhausted at long times which produce larger clusters), but rather fragmentation products of the larger clusters. These points can and have been tested[42] by using focussed and unfocussed ionizing lasers at two energies (5.0 and 6.4 eV) with resulting evidence that fragmentation products are minimized by using the unfocussed ionizing 6.4 eV laser.

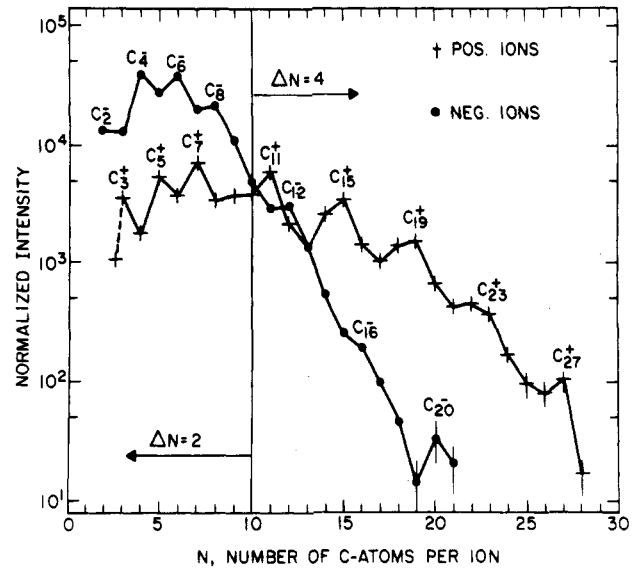

Figure 16. Concentration spectra for $C_n^{\pm}$ as evaporated and quenched[41] and labeled here.

As we discussed previously in connection with shell filling by cap addition or vertex removal with Ar_n^+ clusters (section IIIB), a crossover in structure is usually indicated by a "dead" region (no peaks in c_n) in the concentration spectrum. The measured spectrum[42] for C_n^+ clusters shown in Figure 15 contains such a "dead" region for $30 \leq n \leq 40$. The large n region, with a pronounced peak in c_n at $n = 60$, may correspond to spheroidal (soccer) clusters formed from graphitic fragments. The $n = 60$ polygon contains 60 vertices and 32 faces. A carbon atom placed at each vertex has one double and two single bonds.[43]

The range $10 \leq n \leq 30$ is much better understood. Here there is general agreement[41-44] that the peaks for c_n^+ occur at $n = 4m - 1$, that is, 11, 15, 19, 23 and 27. The period $\Delta n = 4$ is in good agreement with the double-bonded monocyclic ring model.[40]

To obtain spectra for the range $1 \leq n \leq 10$ several techniques have been employed.[41-43] Peaks for c_n^+ at $n = 3$, 5, and 7 have been observed, as shown in Figure 16. This corresponds to stable double-bonded chains. The small value at $n = 9$ can be interpreted as a narrow "dead" region between chains (stable for $n < 8$) and rings (stable for $n > 10$) or it can also be interpreted to indicate that the chain-ring crossover occurs in the range $6 \leq n \leq 8$. In any case the general features of the theoretical chain-and-ring model appear to be well-confirmed by experiment.

Data have also been reported for c_n^- spectra. In one case[41] these closely resemble the $\Delta n = 2$, 4 spectra while in another[43] the similarities are less close. On the whole it appears that because the kinetics of c_n^- formation involve neutral cluster formation followed by electron capture (which itself should be n-dependent), these spectra may be less significant than the c_n^+ spectra.

After this review was completed, a decisive experiment was reported[45] which demonstrates unambiguously the chain-ring transition in C_n^+ clusters at $n = 10$ illustrated in Figure 16. Near 5 eV the photodissociation cross section increases rapidly with cluster size n up to $n = 9$, and then drops abruptly at $n = 10$, where it again begins to rise with increasing n. This behavior is shown in Figure 17. It is clearly the signature of the chain-ring transition predicted 25 years ago by K. Pitzer

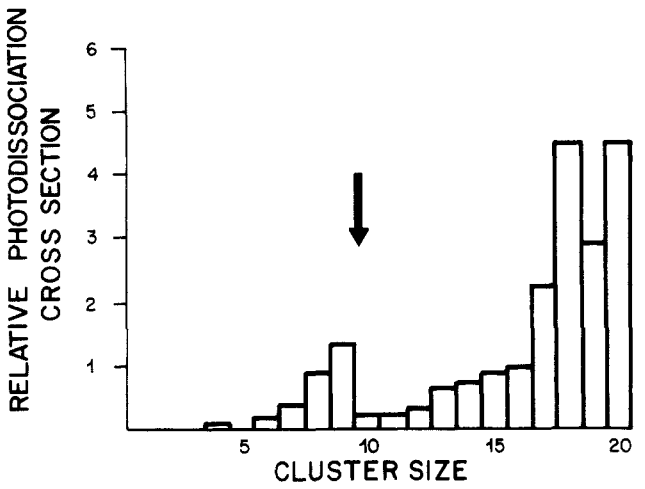

Figure 17. Histogram showing the total photofragmentation cross section for C_n^+ microclusters at 5 eV, with relative uncertainties of 20%. Reprinted with permission from ref 45.

and co-workers.[40] This is the first unambiguous detection of a structural transition (analogous to a bulk phase transition) in vapor-phase microclusters.

VI. Experiment, Computation, and Theory

At this writing (Sept. 1, 1985) the field of microclusters is evolving rapidly and each year sees difficult problems solved with remarkable precision. The complexity of the subject is yielding to the application of many new techniques. At the same time stable microclusters challenge the large-scale computational capabilities of sophisticated quantum theorists. New models of covalent forces spanning wide ranges of bond lengths and bond angles have been constructed which appear to be surprisingly accurate.[35] With practice theorists may become increasingly adept at modelling clusters containing 10 or even 100 or 1000 atoms. Thus the Mackay construction, which has served so well for inert gas clusters, may eventually find analogues in network and even transition metal clusters.

The aim of this thematic review has been to sketch an outline of the interplay between experiment, computation, and theoretical models of the Mackay type for simple systems. Concentration spectra for complex systems have already been measured, and many more undoubtedly will be measured. As in so many other fields of chemistry and physics, much of this data will not be analyzed. It is hoped that this review will clarify by positive examples some of the ingredients useful for analyzing and understanding data in this fascinating field.

References

(1) Conzemius, R. J.; Capellen, J. M. *Int. J. Mass Spect.* **1980**, *34*, 197.
(2) Hopkins, J. B.; Langridge-Smith, P.; Morse, M. D.; Smalley, R. E. *J. Chem. Phys.* **1983**, *78*, 1627.
(3) Bloomfield, L.; Freeman, R.; Brown, W. L. *Phys. Rev. Lett.* **1985**, *54*, 2246.
(4) Soler, J. M.; García, N.; Echt, O.; Sattler, K.; Recknagel, E. *Phys. Rev. Lett.* **1982**, *49*, 1857.
(5) Marlow, W. A. *J. Chem. Phys.* **1980**, *73*, 6284.
(6) Raether, H. *Excitation of Plasmons and Interband Transitions by Electrons*; Springer: New York, 1980.
(7) Mackay, A. C. *Acta Crystallogr.* **1962**, *15*, 916.
(8) Allpress, J. G.; Sanders, J. V. *Aust. J. Phys.* **1970**, *23*, 23.
(9) Echt, O.; Sattler, K.; Recknagel, E. *Phys. Rev. Lett.* **1981**, *47*, 1121.
(10) Hoare, M. R.; Pal, P. *Adv. Phys.* **1971**, *20*, 161.
(11) Milne, T. A.; Greene, F. T. *J. Chem. Phys.* **1967**, *47*, 4095.
(12) Friedman, J.; Beuhler, R. J. *J. Chem. Phys.* **1983**, *78*, 4669.
(13) Ding, A.; Hesslich, J. *Chem. Phys. Lett.* **1983**, *94*, 54.
(14) Harris, I. A.; Kidwell, R. S.; Northby, J. A. *Phys. Rev. Lett.* **1984**, *53*, 2390.
(15) Hoare, M. R. *Adv. Chem. Phys.* **1979**, *40*, 49. Allpress, J. G.; Sanders, J. V. *Surf. Sci.* **1967**, *7*, 1.
(16) Soler, J. M.; Sáenz, J. J.; Garcia, N.; Echt, O. *Chem. Phys. Lett.* **1984**, *109*, 71.
(17) Saile, V.; Skibowski, M.; Steinmann, W.; Gürtler, P.; Koch, E. E.; Kozevnikov, A. *Phys. Rev. Lett.* **1976**, *37*, 305.
(18) Rössler, U. *Phys. Status Solidi* **1970**, *42*, 345.
(19) Farges, J.; Raoult, B.; Rochet, G. *J. Chem. Phys.* **1973**, *59*, 3454. A more recent study [Lee, J. W.; Stein, G. D. *Surf. Sci.* **1985**, *156*, 112] claims to observe a transition from icosahedral to cubic close-packed Ar_n^+ clusters for n near 3000. Again 40 kV electrons used for diffraction may cause fragmentation.
(20) Barker, J. A. *J. Phys. (Lew Ulis, Fr.)* **1977**, *38*, C-2, 37.
(21) Kreisle, D.; Echt, O.; Knapp, M.; Recknagel, E. *Surf. Sci.* **1985**, *156*, 321.
(22) Heine, V.; Weaire, D. *Solid State Phys.* **1970**, *24*, 250; Iñiguez, M. P.; Alonso, J. A.; Balbas, L. C. *Solid State Commun.* **1986**, *57*, 85.
(23) Satter, K., unpublished results.
(24) Pfau, P.; Sattler, K.; Mühlbach, J.; Pflaum, R.; Recknagel, E. *J. Phys. F.* **1982**, *12*, 2131.
(25) Kappes, M. M.; Kunz, R. W.; Schumacher, E. *Chem. Phys. Lett.* **1982**, *91*, 413.
(26) Wigner, E. P.; Seitz, F. *Phys. Rev.* **1933**, *43*, 804.
(27) Knight, W. D.; Clemenger, K.; de Heer, W. A.; Saunders, W. A.; Chou, M. Y.; Cohen, M. L. *Phys. Rev. Lett.* **1984**, *52*, 2141.
(28) Knight, W. D.; de Heer, W. A.; Clemenger, K.; Saunders, W. A. *Solid State Commun.* **1985**, *53*, 445.
(29) Chou, M. Y.; Cleland, A.; Cohen, M. L. *Solid State Commun.* **1984**, *52*, 645.
(30) Clemenger, K. *Phys. Rev. B Condens. Matter* **1985**, *B32*, 1359.
(31) Mühlbach, J.; Pfau, P.; Sattler, K.; Recknagel, E. *Z. Phys. B* **1982**, *B47*, 233.
(32) Somerjai, G. *Chem. Soc. Rev.* **1984**, *13*, 321. Liu, R.; Ehrlich, G. *Surf. Sci.* **1982**, *119*, 207.
(33) Whetten, R. L.; Cox, D. M.; Trevor, D. J.; Kaldor, A. *Phys. Rev. Lett.* **1985**, *54*, 1494.
(34) Geusic, M. F.; Morse, M. D.; Smalley, R. E. *J. Chem. Phys.* **1985**, *82*, 590. Martin, T. P.; Schaber, H. *J. Chem. Phys.* **1985**, *83*, 855.
(35) Raghavachari, K.; Logovinsky, V. *Phys. Rev. Lett.* **1985**, *55*, 2853. Biswas, R.; Hamann, D. R. *Phys. Rev. Lett.* **1985**, *55*, 2001. Tomânek, D.; Schlüter, M. A. *Phys. Rev. Lett.* **1986**, *56*, 1055.
(36) Bloomfield, L. A.; Freeman, R. R.; Brown, W. L.; *Phys. Rev. Lett.* **1985**, *54*, 2246 and unpublished results. Heath, J. R.; Lee, Y.; O'Brien, S. C.; Zhang, Q.-L.; Curl, R. F.; Tittel, F. K.; Smalley, R. E. *J. Chem. Phys.* **1985**, *83*, 3330.
(37) Cohen, B. L. *Phys. Rev.* **1960**, *120*, 925.
(38) Phillips, J. C. *J. Chem. Phys.* **1985**, *83*, 3330; *Phys. Today*, **1982**, *35* (Feb), 1.
(39) Phillips, J. C. *Bonds and Bands in Semiconductors*; Academic: New York, 1973; p 94, p 204.
(40) Strickler, S. J.; Pitzer, K. S. In *Molecular Orbitals in Chemistry* Pullman, B., Löwdin, P. O., Eds. Academic: New York, 1964; p 281.
(41) Fürstenau, N.; Hillenkamp, F. *Int. J. Mass Spectrom.* **1981**, *37*, 155.
(42) Rohlfing, E. A.; Cox, D. M.; Kaldor, A. *J. Chem. Phys.* **1984**, *81*, 3322.
(43) Kroto, H. W.; Heath, J. R.; O'Brien, S. C.; Carl, R. F.; Smalley, R. E. *Nature* **1985**, *318*, 162.
(44) Bloomfield, L. A.; Geusic, M. E.; Freeman, R. R.; Brown, W. L., unpublished results.
(45) Geusic, M. E.; Jarrold, M. F.; Freeman, R. R., unpublished results.